iScience

CellPress
OPEN ACCESS

Article

ERK1-mediated immunomodulation of mesenchymal stem cells ameliorates inflammatory disorders

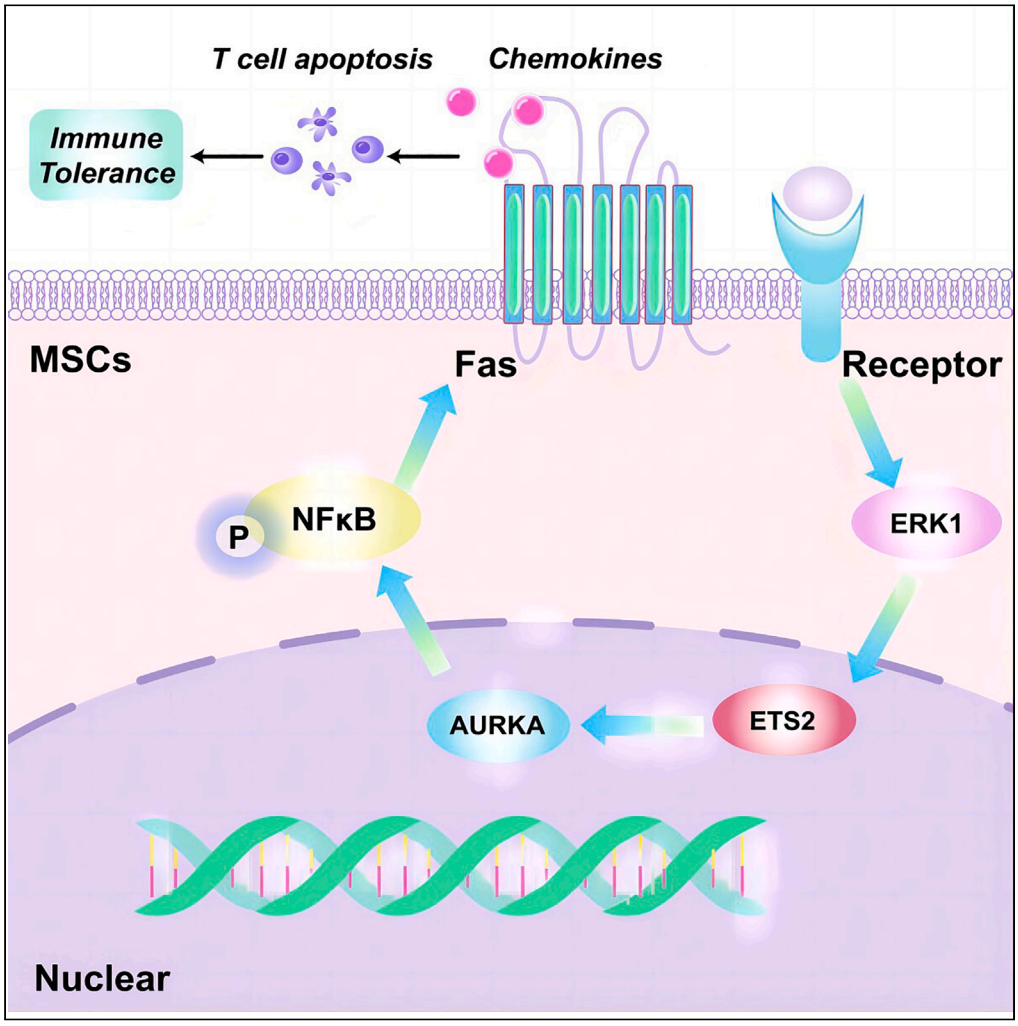

Qing Zhang, Xiao Lei, Fang Wang, ..., Fang Jin, Chider Chen, Bei Li

chenc10@upenn.edu (C.C.)
libei2021@fmmu.edu.cn (B.L.)

Highlights

ERK1 mediates MSC function in promoting T cell apoptosis & reducing Th17/Treg ratio

ERK1 promoting the immunoregulation ability via ERK1/ETS2/AURKA/NF-κB/Fas cascade

LA-treated MSCs systemic infusion effectively alleviates autoimmune disease symptoms

Zhang et al., iScience 26, 107868
October 20, 2023
https://doi.org/10.1016/j.isci.2023.107868

iScience

CellPress
OPEN ACCESS

Article

ERK1-mediated immunomodulation of mesenchymal stem cells ameliorates inflammatory disorders

Qing Zhang,[1,2,3,7] Xiao Lei,[1,3,7] Fang Wang,[5,7] Xiaoning He,[1] Lu Liu,[1,3] Yuxia Hou,[2] Yuan Liu,[6] Fang Jin,[3] Chider Chen,[4,*] and Bei Li[1,8,*]

SUMMARY

Immune system disorders, especially T cell disorders, are important therapeutic targets of mesenchymal stem cells (MSCs) in many autoimmune diseases (ADs). Although extracellular regulated protein kinases (ERKs) play a role in MSC therapy by promoting T cell apoptosis, the mechanism remains unclear. Our findings indicate that *ERK1*$^{-/-}$ bone marrow MSCs (BMMSCs), but not *ERK2*$^{-/-}$ BMMSCs, failed to promote T cell apoptosis due to incapacity to activate the ETS2/AURKA/NF-κB/Fas/MCP-1 cascade. Moreover, *ERK1*$^{-/-}$ BMMSCs were unable to upregulate regulatory T cells and suppress T helper 17 cells. Licochalcone A (LA), which promotes ERK pathway activation, enhanced the therapeutic efficacy of MSC therapy in ulcerative colitis and collagen-induced arthritis mice. Our findings suggest that ERK1, but not ERK2, plays a crucial role in regulating T cells in MSCs. LA-treated MSCs provide a strategy to improve the efficacy of MSC-based treatments for ADs.

INTRODUCTION

The overall prevalence of autoimmune diseases (ADs) in the general population is approximately 3%–5%.[1,2] Rheumatoid arthritis (RA) and ulcerative colitis (UC) are typical ADs that exhibit high morbidity in different racial groups.[3] Drugs commonly used to treat ADs are associated with side effects and high recurrence rates and may even be ineffective for some patients.[4] As a result, developing more effective therapeutic approaches with fewer side effects for ADs remains a challenge.

Systemic infusion of mesenchymal stem cells (MSCs) has been shown to treat ADs by regulating the immune system.[5–7] To date, more than 100 clinical trials of MSC therapy (MSCT) for ADs have been conducted worldwide, including more than 10 trials for RA and UC. Although MSCT has achieved a certain therapeutic effect in some trials, there have also been some reports of poor efficacy. For example, in a clinical study in which MSCs were used to treat resistant RA, 28 patients reported a good or moderate response, while 24 patients reported no response after 48 weeks[8] In another clinical trial, MSCT showed no effect on systemic lupus erythematosus (SLE) activity over 14 weeks.[9] These clinical trial results indicate that MSCT is relatively safe for ADs, but its efficacy is inconsistent. Thus, the mechanism of MSCT should be clarified to improve its efficacy.

The immunoregulatory effects of MSCs on adaptive immunity are manifested through their immunosuppressive action on T cells. Previous studies have indicated that the extracellular regulated protein kinase (ERK) cascade regulates various aspects of the immune system, including immune cell function, and plays a crucial role in autoimmune responses. Evidence suggests that the ERK pathway regulates immunosuppression by reducing the Th17/Treg ratio.[10–12] Moreover, several small molecular compounds, such as sesamin,[13] 2-(2-mercaptoethanol)-3-methyl-1,4-napthoquinone,[14] brain-derived neurotrophic factor,[15] and concentrated growth factor,[16] have been reported to activate the ERK pathway in the treatment of periodontitis and ADs such as UC. However, whether regulating the ERK pathway can enhance MSCT efficacy for AD treatment remains largely unexplored.

In this study, we discover an unrecognized mechanism where ERK1, but not ERK2, is essential for MSC-induced T cell apoptosis. ERK1 modulates MSC-based T cell regulation through the ERK1/E26 transformation-specific sequence 2/aurora A kinase/nuclear factor kappa B/Fas (ERK1/ETS2/AURKA/NF-κB/Fas) cascade. Furthermore, treatment of human MSCs with licochalcone A (LA), which upregulates ERK1 expression, demonstrates better therapeutic effects of MSCT on UC and RA. Our findings suggest that intracellular activation of ERK1

[1]State Key Laboratory of Oral & Maxillofacial Reconstruction and Regeneration & National Clinical Research Center for Oral Diseases & Shaanxi International Joint Research Center for Oral Diseases, Center for Tissue Engineering, School of Stomatology, the Fourth Military Medical University, Xi'an, Shaanxi 710032, China
[2]Key Laboratory of Shaanxi Province for Craniofacial Precision Medicine Research, College of Stomatology, Xi'an Jiaotong University, Xi'an, Shaanxi 710004, China
[3]Shannxi Clinical Research Center for Oral Diseases & Department of Orthodontics, School of Stomatology, the Fourth Military Medical University, Xi'an, Shaanxi 710032, China
[4]Department of Oral and Maxillofacial Surgery and Pharmacology, School of Dental Medicine, University of Pennsylvania, Philadelphia, PA 19104, USA
[5]Department of Blood Purification, General Hospital of Central Theater Command of PLA, 68 Huangpu Road, Wuhan, Hubei 430010, China
[6]The Affiliated Northwest Women's and Children's Hospital of Xi'an Jiaotong University Health Science Center, Xi'an, Shaanxi 710061, China
[7]These authors contributed equally
[8]Lead contact
*Correspondence: chenc10@upenn.edu (C.C.), libei2021@fmmu.edu.cn (B.L.)
https://doi.org/10.1016/j.isci.2023.107868

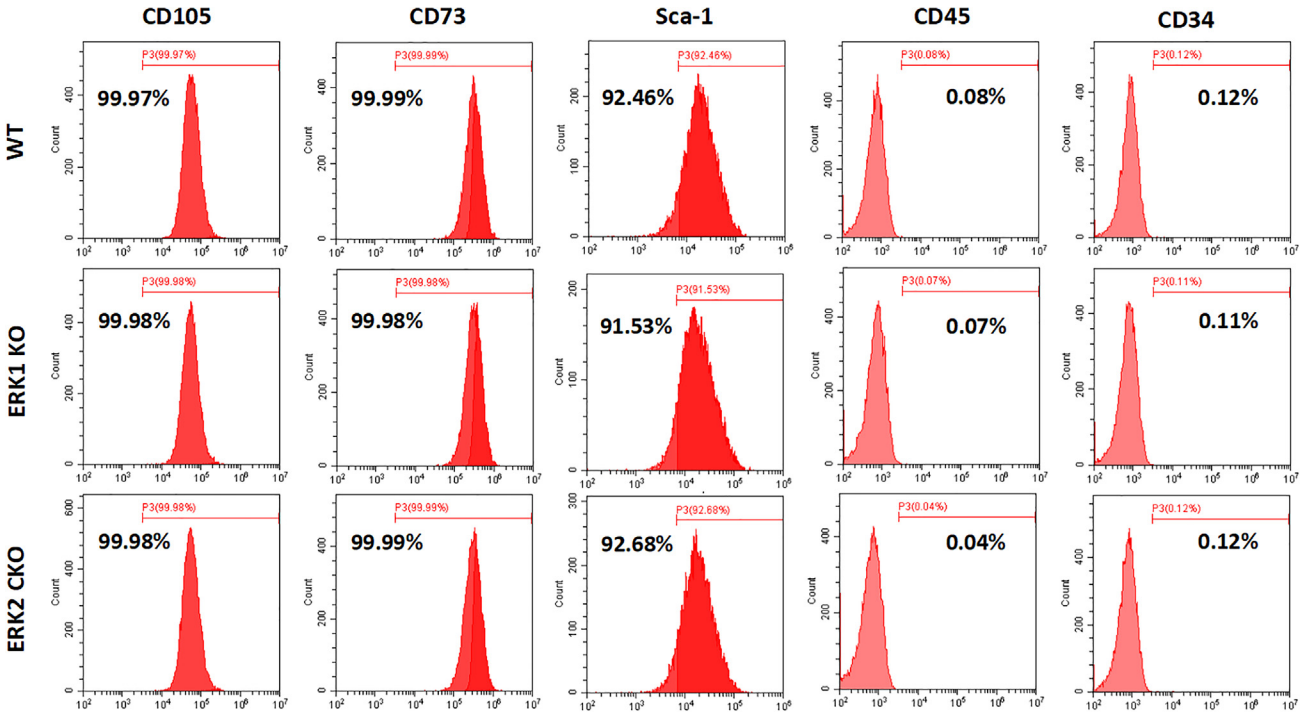

Figure 1. Flow cytometric characterization of BMMSCs

Flow cytometric analysis of ex vivo-expanded WT mouse BMMSCs, ERK1 KO mouse BMMSCs, and ERK2 CKO mouse BMMSCs.

via LA treatment enhances the immunomodulatory ability of MSCs, providing a strategy to improve the therapeutic efficiency of MSCT for ADs.

RESULTS

ERK1 governs immunomodulatory properties of MSCs

To determine the isoform of ERK signaling involved in MSC-based immunomodulation, purified wild-type (WT), *ERK1*$^{-/-}$, and *ERK2*$^{-/-}$ bone marrow MSCs (BMMSCs) were successfully obtained from mouse bone marrow. BMMSCs showed positive expression (≥99% positive) of CD105, CD73, and Sca-1 and negative expression (<1% positive) of CD45 and CD34 (Figure 1). Next, WT, *ERK1*$^{-/-}$, and *ERK2*$^{-/-}$ BMMSCs were systemically infused into 3% dextran sodium sulfate (DSS)-induced colitis mice at 3 days post-DSS induction (Figure 2A). Colitis mice showed significantly reduced body weight from days 5–10 post-DSS induction compared with control mice. However, after infusion of either WT or *ERK2*$^{-/-}$ BMMSCs, but not *ERK1*$^{-/-}$ BMMSCs, the body weight of colitis mice was partially rescued at 10 days post-DSS induction (Figure 2B). The disease activity index (DAI) was significantly higher in colitis mice than in control mice. After infusion with WT or *ERK2*$^{-/-}$ BMMSCs, the DAI was decreased, while *ERK1*$^{-/-}$ BMMSCs infusion failed to reduce the DAI (Figure 2C). Histological analysis revealed the absence of an epithelial layer and infiltration of inflammatory cells in the colon of mice in the DSS and *ERK1*$^{-/-}$ groups. However, colitis mice receiving WT or *ERK2*$^{-/-}$ BMMSCs showed recovery of the colon epithelial structure and elimination of inflammatory cells (Figures 2D and 2E). Both WT and *ERK2*$^{-/-}$ BMMSCs, but not *ERK1*$^{-/-}$ BMMSCs, significantly upregulated Tregs and downregulated Th17 cells (Figures 2F and 2G and S1A and S1B). These findings indicate that the infusion of *ERK1*$^{-/-}$ BMMSCs failed to regulate immunomodulation, suggesting that ERK1 is essential for MSC-based immunotherapy for colitis.

ERK1 regulates MSC-based T cell regulation by activating Fas

In our previous study, we showed that MSCs were capable of inducing T cell apoptosis through the Fas/FasL signaling pathway.[17,18] To investigate whether Fas/FasL signaling contributes to the deficiency of *ERK1*$^{-/-}$ BMMSCs-mediated immunomodulation, we conducted a BMMSCs/T cell co-culture experiment to examine the immunomodulatory properties of *ERK1*$^{-/-}$ BMMSCs. Flow cytometric analysis showed that *ERK1*$^{-/-}$ BMMSCs had a significantly reduced capacity to induce T cells apoptosis compared with WT and *ERK2*$^{-/-}$ BMMSCs (Figures 3A and S1C). We next examined the expression levels of Fas and FasL using western blotting and found that Fas, but not FasL, was significantly downregulated in *ERK1*$^{-/-}$ BMMSCs (Figures 3B and 3C). Since Fas controls chemokine release to recruit T cells to initiate an interplay between MSCs and activated T cells,[18] we employed an *in vitro* transwell co-culture system. In this system, activated T cells migrated to either WT or *ERK2*$^{-/-}$ BMMSCs to initiate cell-cell contact-induced apoptosis. However, *ERK1*$^{-/-}$ BMMSCs exhibited a significantly reduced capacity to recruit activated T cells compared with WT or *ERK2*$^{-/-}$ BMMSCs.

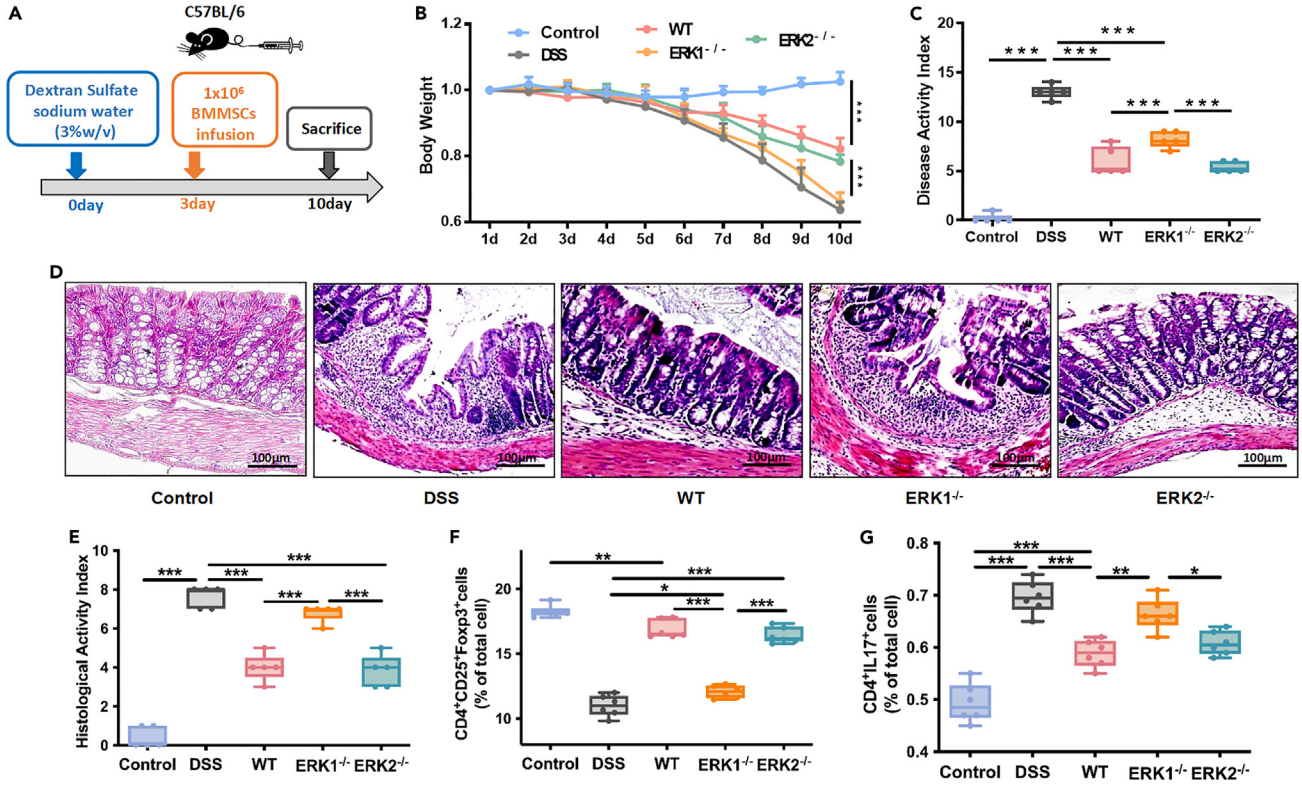

Figure 2. The therapeutic efficacy of *ERK1*$^{-/-}$ BMMSCs on DSS mice was limited

(A) Schema indicating of the study design.

(B) The relative changes of body weight.

(C) Disease activity index was determined according to the symptoms of colitis.

(D, E) Histological changes of colon were determined by H&E staining and presented in column.

(F) Tregs frequencies were evaluated by flow cytometric analysis and presented in column.

(G) Th17 frequencies were evaluated by flow cytometric analysis and presented in column. n = 6. Comparisons between means groups were analyzed using ordinary one-way ANOVA with Tukey's multiple comparisons test. Bars show mean ± SEM. Statistical significance is indicated with *p < 0.05, **p < 0.01, ***p < 0.001. Scale bars = 100 μm. BMMSCs, bone marrow derived mesenchymal stem cells; DSS, dextran sodium sulfate.

Fas$^{-/-}$ BMMSCs were used as a comparative control, which showed a reduced ability to recruit activated T cells in the transwell co-culture system (Figures 3D and 3E). Since Fas initiates interplay between MSCs and activated T cells by controlling chemokine release,[18] we investigated the differences in cytokines released by WT, *ERK1*$^{-/-}$, and *ERK2*$^{-/-}$ BMMSCs. Analysis of cytokine array data showed that *ERK1*$^{-/-}$ BMMSCs expressed reduced levels of monocyte chemotactic protein-1 (MCP-1), a member of the C-C motif chemokine family and a T cell chemoattractant cytokine (Figures 3F and 3G). Furthermore, we confirmed that MCP-1 levels were significantly reduced in the *ERK1*$^{-/-}$ BMMSCs culture supernatant (Figure 3H).

ERK1 regulates MSC-based T cell regulation through the ETS2/AURKA/NFκB cascade

Since nuclear factor κB (NF-κB) plays a critical role in regulating *Fas* transcription,[19] we examined the expression levels of NF-κB signaling network members. Western blotting revealed that the expression levels of phosphorylated NF-κB (*p*-NFκB) and phosphorylated inhibitor of kappaB (*p*-IκB), but not phosphorylated IκB kinase (*p*-IKK), were downregulated in *ERK1*$^{-/-}$ BMMSCs (Figures 4A and 4C). Given that IKK did not affect *p*-NFκB in *ERK1*$^{-/-}$ BMMSCs, we next examined the expression levels of another kinase, AURKA, known to phosphorylate IκB and induce the nuclear translocation of NF-κB.[20,21] Western blotting revealed that the expression levels of both phosphorylated AURKA (*p*-AURKA) and total AURKA were decreased in *ERK1*$^{-/-}$ BMMSCs (Figures 4B and 4C). These data prompted us to examine the promoter region of *aurka* using the PROMO search tool. We identified four candidate sites (ETS2-1–ETS2-4) for ETS2, a downstream molecule of the ERK signaling pathway, which closely matched with ETS2 transcription factor consensus targets. Western blotting revealed that the ETS2 levels were dramatically decreased in *ERK1*$^{-/-}$ BMMSCs (Figures 4B and 4C). To determine whether decreased expression of AURKA is associated with the alteration of the ERK1/ETS2 signaling in *ERK1*$^{-/-}$ BMMSCs, we generated an *aurka* promoter reporter construct, in which the defined region of the *aurka* promoter and the flanking region were placed upstream of a reporter gene encoding firefly luciferase. We found that *aurka* promoter activity was

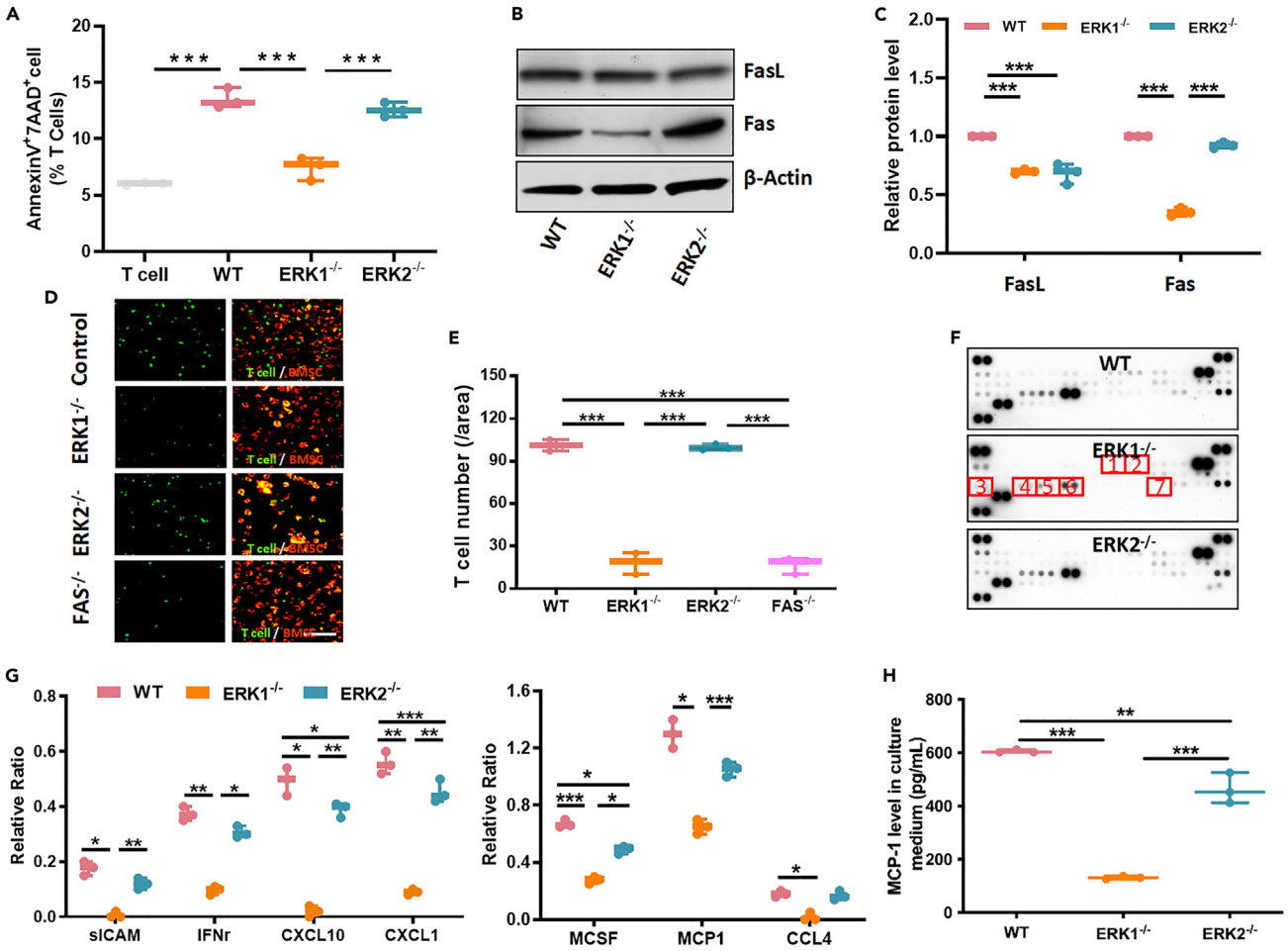

Figure 3. Decreased MCP-1 released by *ERK1*$^{-/-}$ BMMSCs resulted in the decreased T cells apoptosis

(A) The apoptotic activated T cells were evaluated by flow cytometric analysis and presented in column.

(B) Fas and FasL expressions were detected by western blot analysis.

(C) The relative expressions of Fas and FasL were presented in column.

(D and E) Recruitment of activated T cells (red) by BMMSCs (green).

(F) Chemokines levels were detected by cytokine array analysis.

(G) The relative ratios of chemokines were presented in column.

(H) MCP-1 levels of culture supernatants were revealed by ELISA analysis and presented in column. Comparisons between means groups were analyzed using ordinary one-way ANOVA with Tukey's multiple comparisons test. Bars show mean ± SEM. Statistical significance is indicated with *p < 0.05, **p < 0.01, ***p < 0.001. Scale bars = 50 μm. BMMSCs, bone marrow derived mesenchymal stem cells; MCP-1, monocyte chemotactic protein-1.

markedly reduced in *ERK1*$^{-/-}$ BMMSCs. Moreover, when *ERK1*$^{-/-}$ BMMSCs were transfected with a reporter vector, the luciferase assay showed significantly decreased *aurka* promoter activity. These results prompted us to examine whether ETS2-bound DNA at the predicted sites were significantly enriched in *ERK1*$^{-/-}$ BMMSCs. By employing a chromatin immunoprecipitation (ChIP) assay, we identified that the ETS2 binding consensus sequences within the promoter region recruited ETS2. The ChIP assay showed that ETS2-bound DNA at the ETS2-2 and ETS2-3 candidate sites, but not that at ETS2-1 and ETS2-4 sites, was significantly depleted in *ERK1*$^{-/-}$ BMMSCs, suggesting that ETS2 acts as an initiator to elevate AURKA expression (Figure 4D). Introduction of ETS2 mutated at the ETS2-2 and ETS2-3 candidate sites markedly diminished the expression of the *aurka*-luciferase reporter in both WT and *ERK2*$^{-/-}$ BMMSCs, indicating the direct initiation of AURKA expression by the ERK1/ETS2 cascade (Figure 4E). In summary, ERK1 regulates MSC-based immunomodulation through the ETS2/AURKA/NF-κB cascade (Figure 4F).

LA-treated umbilical cord mesenchymal stem cells (UCMSCs) improved MSCT efficiency in DSS-induced colitis mice

A previous study demonstrated that LA promoted, while U0126 inhibited, the expression of phosphorylated ERK (*p*-ERK).[22,23] We verified whether the expression levels of proteins related to the ERK cascade in human UCMSCs were affected by LA (LA-UCMSC group) or U0126 (U0126-UCMSC group) treatment. Purified UCMSCs were successfully obtained from human umbilical cords. We found positive

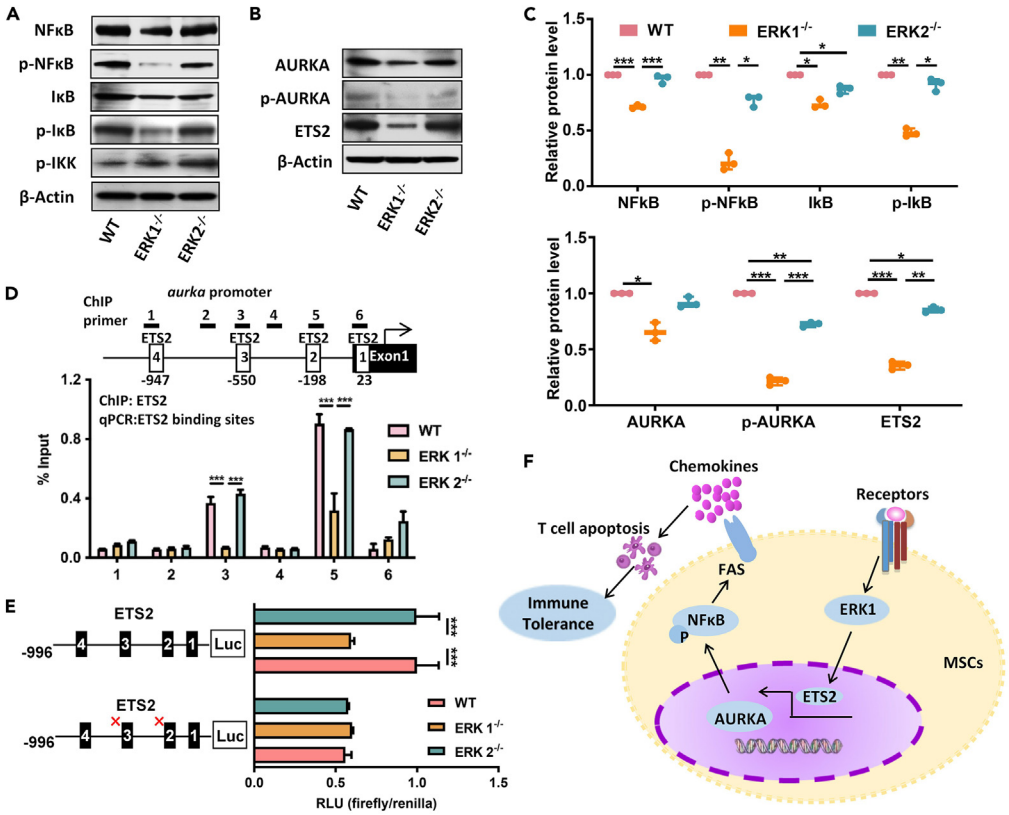

Figure 4. ERK1 governs immunomodulatory properties of MSCs via ETS2/AURKA/NF-κB signaling

(A) NF-κB, *p*-NFκB, IKB, *p*-IKB, and *p*-IKK expression levels were detected by western blot analysis.

(B) AURKA, *p*-AURKA, and ETS2 expression levels were detected by western blot analysis.

(C) The relative levels of proteins were presented in column.

(D) Promoter regions of *aurka* were examined by PROMO search tools, and ETS2-bound DNA sites were identified by ChIP assay.

(E) *aurka* promoter activities were measured by luciferase assay, and relative light unit was presented in column.

(F) Schema indicating of the ERK1/ETS2/AURKA/NF-κB/Fas cascade. Comparisons between means groups were analyzed using ordinary one-way ANOVA with Tukey's multiple comparisons test. Bars show mean ± SEM. Statistical significance is indicated with *p < 0.05, **p < 0.01, ***p < 0.001.

expression (≥99% positive) of CD105, CD90, and CD73 and negative expression (<1% positive) of CD45, CD34, CD14, CD19, and HLA-DR (Figure 5A). Additionally, *p*-ERK, Fas, *p*-NFκB, and *p*-IKB, but not total ERK, FasL, total NF-κB, or total IKB, were significantly upregulated in LA-UCMSCs. On the contrary, the expression of *p*-ERK, *p*-NFκB, and *p*-IKB was reduced in U0126-UCMSCs (Figures 5B–5D). Next, to examine the immunomodulatory properties of LA-UCMSCs and U0126-UCMSCs, we conducted a UCMSCs/T cells co-culture experiment. Flow cytometric analysis showed that, compared with control UCMSCs, U0126-UCMSCs had a significantly reduced capacity to induce T cell apoptosis, whereas LA-UCMSCs had a remarkably increased capacity to induce T cell apoptosis (Figures 5E and S2A).

As LA treatment improved the capacity of UCMSCs to induce T cell apoptosis, we investigated whether LA treatment enhanced MSCT efficiency. UCMSCs, LA-treated UCMSCs, and U0126-treated UCMSCs were systemically infused into DSS-induced experimental colitis mice at 3 days post-DSS induction (Figure 6A). Colitis mice displayed significantly reduced body weight from days 6–10 post-DSS induction compared with control mice. After infusion of either UCMSCs or U0126-treated UCMSCs, the body weight of colitis mice was partially rescued at 10 days post-DSS induction. However, after infusion of LA-treated UCMSCs, the body weight of colitis mice was remarkably rescued at 10 days post-DSS induction (Figure 6B). The DAI was significantly elevated in colitis mice compared with that in control mice. After the infusion of UCMSCs or U0126-treated UCMSCs, the DAI was decreased in colitis mice, whereas, the DAI decreased significantly with the infusion of LA-treated UCMSCs (Figure 6C). Histological analysis of colon tissues from each group revealed an absence of an epithelial layer and infiltration of inflammatory cells in mice in the DSS and U0126-UCMSC groups. However, colitis mice that received UCMSCs or LA-treated UCMSCs showed a recovery of the epithelial structure and partial elimination of inflammatory cells (Figures 6D and 6E). Regarding the immune regulation, colitis mice had decreased Tregs and elevated Th17 cells on 10 days post-DSS induction. LA-treated UCMSCs increased the percentage of Tregs cells and reduced the percentage of Th17 cells compared with control and U0126-UCMSC group mice (Figures 6F, 6G, S2B, and S2C).

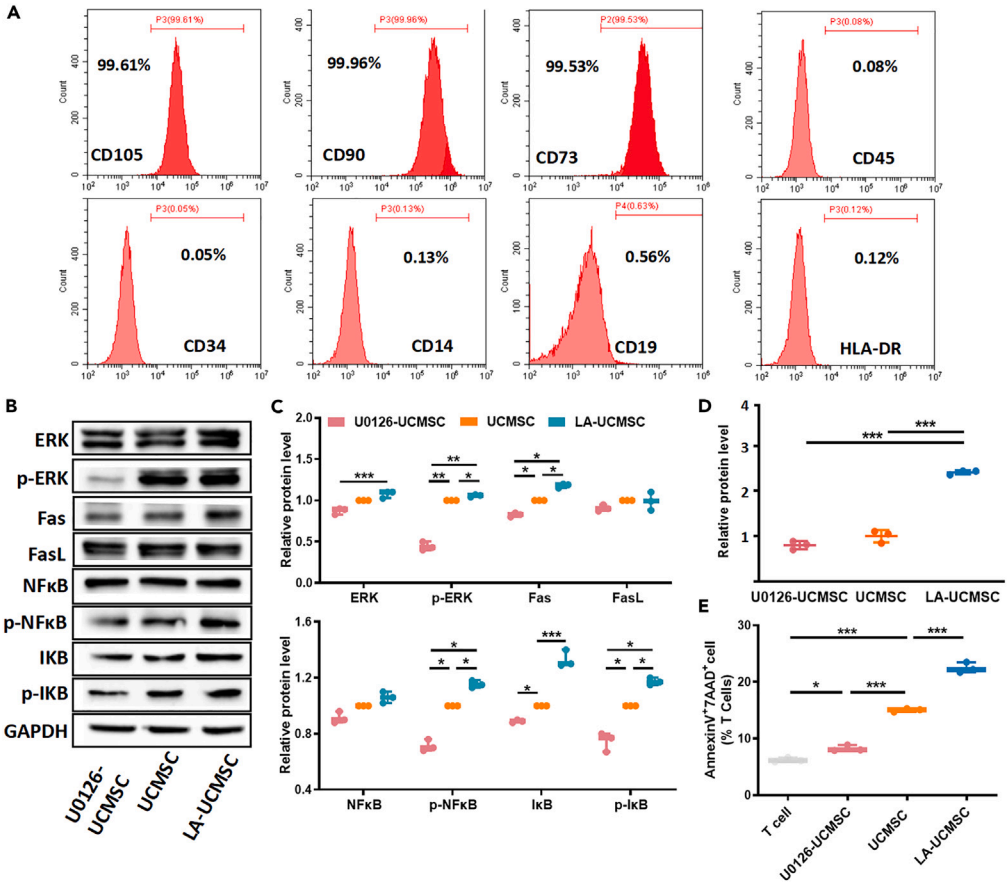

Figure 5. LA improved MSC-based immune regulation via ERK/Fas signaling

(A) Flow cytometric analysis of ex vivo-expanded human UCMSCs.

(B) The expressions of ERK cascade relative proteins were detected by western blot.

(C) The relative levels of proteins were presented in column.

(D) The relative expressions of *p*-ERK proteins were detected by flow cytometry.

(E) The apoptotic activated T cells were evaluated by flow cytometric analysis and presented in column. Comparisons between means groups were analyzed using ordinary one-way ANOVA with Tukey's multiple comparisons test. Bars show mean ± SEM. Statistical significance is indicated with *p < 0.05, **p < 0.01, ***p < 0.001. LA, Licochalcone A; MSCs, mesenchymal stem cells.

LA-treated UCMSCs showed improved MSCT efficiency for collagen-induced arthritis (CIA) mice

To further confirm that LA treatment is an effective and stable method to improve MSCT efficacy for ADs, we used LA-treated UCMSCs to treat another AD model, CIA mice. UCMSCs, LA-treated UCMSCs, and U0126-treated UCMSCs were systemically infused into CIA mice at 30 days after the initial collagen injection (Figure 7A). The severity score was recorded every 3 days after MSC treatment. CIA mice exhibited significantly increased severity scores compared with control mice. After the infusion of either UCMSC or U0126-treated UCMSCs, the severity score of CIA mice was partially rescued, whereas the infusion of LA-treated UCMSCs resulted in the most substantial reduction of the severity score (Figure 7B). To determine the severity of arthritis, we performed micro-computed tomography (micro-CT) analysis to measure the bone shape and volume (Figure 7C). CIA mice showed a rough and irregular articular appearance of the joint surfaces, with a diffuse lesion pattern. However, the number of lesions was lower in the UCMSC and U0126-UCMSC groups. The articular appearance in the LA-UCMSC group closely resembled that of the control group. Quantitative analysis of the micro-CT images revealed that mice in the LA-UCMSC group presented the highest bone volume, except for control mice. In contrast, mice in the U0126-UCMSC group presented a lower bone volume compared with those in the UCMSC group (Figure 7D). Histopathological examination of mouse ankles was conducted to determine cartilage destruction and inflammation (Figure 7E). In CIA mice, cartilage and bony structure destruction were observed on the articular surfaces of the joint. In addition, synovial hyperplasia and inflammatory cell infiltration were observed on the articular surfaces of the joints of CIA mice. Mice in the LA-UCMSC group showed less bone/cartilage destruction and inflammatory cell infiltration than those in the UCMSC and U0126-UCMSC groups (Figure 7F). Regarding the immune regulation, CIA mice had decreased Tregs and elevated Th17 cells. LA-treated UCMSCs exhibited more powerful capacity to upregulate Tregs and downregulate Th17 cells than WT and U0126-treated UCMSCs (Figures 7G, 7H, S2D, and S2E).

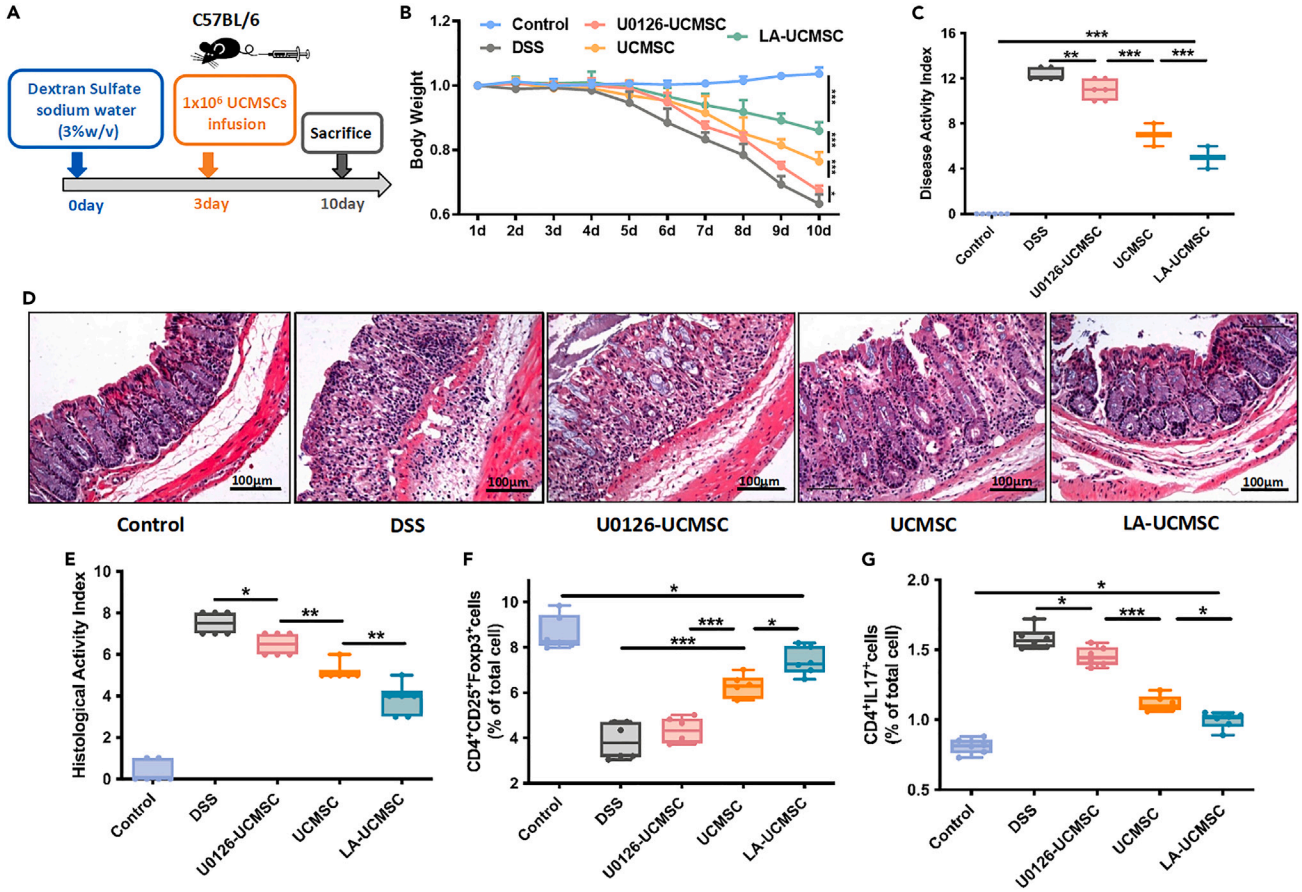

Figure 6. LA-treated UCMSCs improved MSCT efficiency on DSS-induced colitis mice

(A) Schema indicating of the study design.

(B) The relative changes of body weight.

(C) Disease activity index was determined according to the symptoms of colitis.

(D, E) Histological changes of colon were determined by H&E staining and presented in column.

(F) Tregs frequencies were evaluated by flow cytometric analysis and presented in column.

(G) Th17 frequencies were evaluated by flow cytometric analysis and presented in column. n = 6. Comparisons between means groups were analyzed using ordinary one-way ANOVA with Tukey's multiple comparisons test. Bars show mean ± SEM. Statistical significance is indicated with *p < 0.05, **p < 0.01, ***p < 0.001. Scale bars = 100 μm. LA, Licochalcone A; UCMSCs, umbilical cord mesenchymal stem cells; MSCT, mesenchymal stem cells therapy; DSS, dextran sodium sulfate.

DISCUSSION

In this study, we discovered an unrecognized mechanism whereby ERK1, but not ERK2, is essential in MSC-induced T cell apoptosis. ERK1 modulates MSC-based T cell regulation through the ERK1/ETS2/AURKA/NF-κB/Fas cascade. Furthermore, LA treatment, which upregulates ERK1 expression in MSCs, could potentially improve MSCT efficiency for ADs.

For ADs, researchers and doctors have been working to develop new therapeutic approaches, such as gene therapy and MSCT. The drawbacks of gene therapy in ADs mainly include toxicity of the vector, insufficient transduction efficiency of target cells, inconsistent expression of the transgene, putative aberrant expression near integration sites raising safety issues, and lack of long-term expression of the transgene. The above problems limit the clinical application of gene therapy in ADs to some extent.[24,25] It is well-accepted that MSCs promote T lymphocyte apoptosis and govern immunomodulation. However, the exact mechanism underlying the regulatory effect of MSCs on immunity remains unclear. In our previous studies, ERK was associated with MSC-mediated T lymphocyte apoptosis and inflammatory regulation. Although ERK1 and ERK2 share 83% of the homologous amino acids, they are encoded by different genes and have distinct functions.[26,27] Particularly, we aimed to investigate whether ERK1 and ERK2 performed different functions in inhibiting T cells and regulating immunity. Our findings revealed that WT and *ERK2*$^{-/-}$ BMMSCs showed similar MSCT efficiency, whereas *ERK1*$^{-/-}$ BMMSCs had almost no treatment effect on DSS mice, indicating that ERK1, but not ERK2, participates in the immunomodulation of MSCT for ADs.

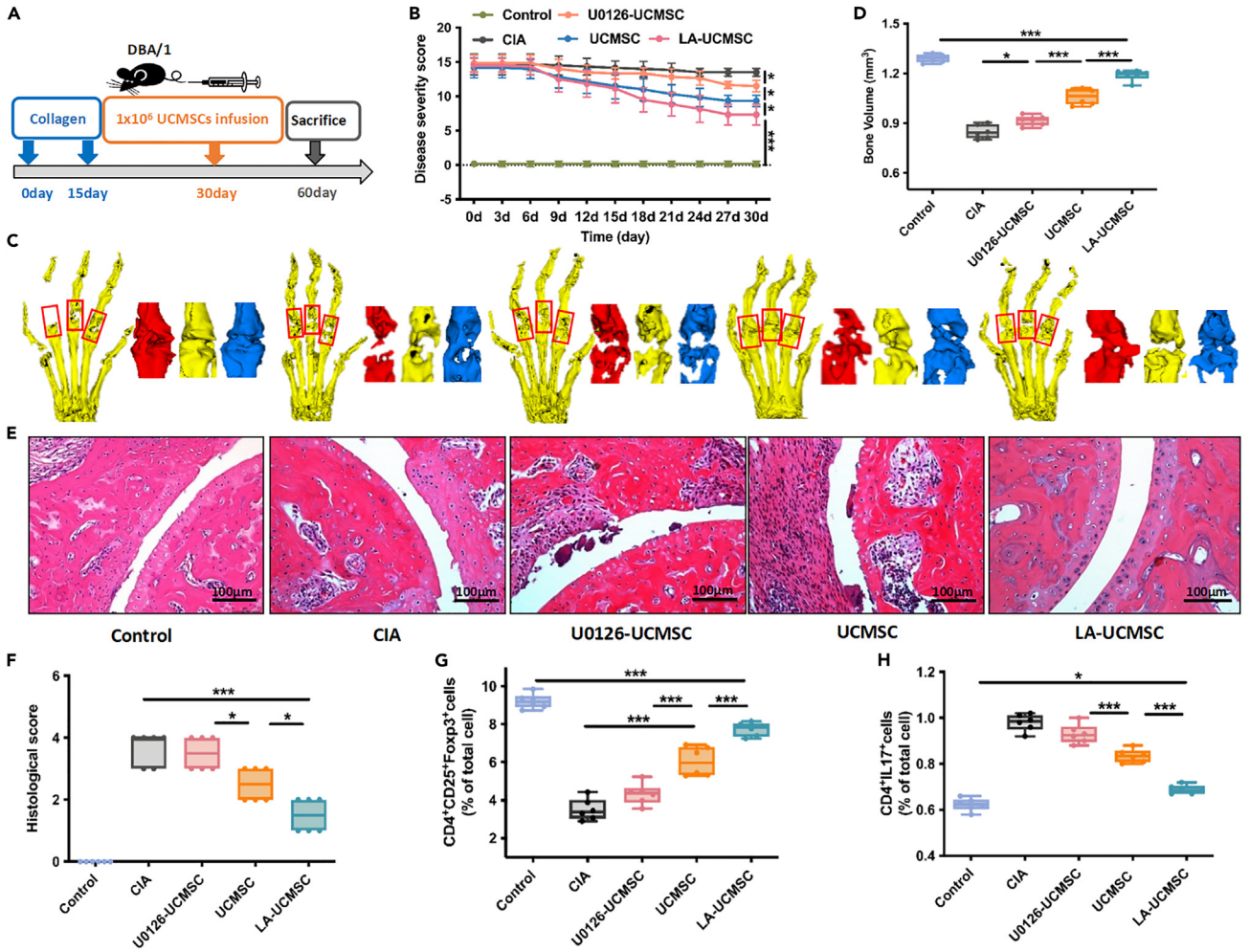

Figure 7. LA-treated UCMSCs improved MSCT efficiency on CIA mice

(A) Schema indicating of the study design.

(B) Disease activity index was determined according to the symptoms of rheumatoid arthritis.

(C) Joint bone surface structures and bone volumes were determined by micro-CT.

(D) Joint bone volumes were measured and presented in column.

(E and F) Histological changes of joint were determined by H&E staining and presented in column.

(G) Tregs frequencies were evaluated by flow cytometric analysis and presented in column.

(H) Th17 frequencies were evaluated by flow cytometric analysis and presented in column. n = 6. Comparisons between means groups were analyzed using ordinary one-way ANOVA with Tukey's multiple comparisons test. Bars show mean ± SEM. Statistical significance is indicated with *p < 0.05, ***p < 0.001. Scale bars = 100 μm. LA, Licochalcone A; UCMSCs, umbilical cord mesenchymal stem cells; MSCT, mesenchymal stem cells therapy; CIA, collagen-induced arthritis.

Evidence indicates that the ERK pathway in MSCs is involved in the immunosuppressive effect of MSCs in the treatment of RA and SLE.[28,29] Upon *in vivo* application, the activation of the ERK pathway is essential for the motility, adhesion, proliferation, and differentiation potential of MSCs.[28,30,31] In addition, the ERK pathway is involved in the regulation of FasL expression.[22] MSCs have been shown to suppress T cell activation and proliferation via Fas-mediated apoptosis.[32] Our previous study revealed that both Fas and FasL signaling pathways participate in MSC-induced T cell apoptosis.[18] In this study, we demonstrated that ERK is involved in Fas expression in MSCs and further distinguished the roles of ERK1/2 subtypes, confirming that ERK1, rather than ERK2, is associated with Fas expression and Fas-induced T cell apoptosis of MSCs.

Enhanced phosphorylation of ERK and IκB is accompanied by NF-κB activation and Fas expression in human MSCs, enhancing their immunosuppressive ability.[33,34] The IKK/IκB/NF-κB pathway is the most classical upstream pathway of Fas expression. However, we did not observe a significant change in IKK phosphorylation levels in *ERK1*$^{-/-}$ and *ERK2*$^{-/-}$ MSCs. Previous studies have reported that although IKK is involved in the immunosuppressive ability of MSCs, it is not the only component involved.[35] Knockout of *IKK* did not reduce the immunosuppressive ability of MSCs.[36] Therefore, we screened AURKA, another accepted upstream regulator of IκB/NF-κB, and examined the expression and phosphorylation levels of AURKA and IκB in *ERK1*$^{-/-}$ and *ERK2*$^{-/-}$ MSCs. AURKA not only phosphorylated IκB but also acted as a

downstream target of ERK.[20,37] The results showed that IκB, but not IKK, was phosphorylated by AURKA, indicating that IKK does not participate in the immunoregulatory function of MSCs.

ETS2, a member of the ETS-domain family, acts as both the downstream target of ERK and the upstream regulator of AURKA.[37,38] In MSCT, ETS genes have been reported as targets for the protection and regeneration of cardiac muscle and bone matrix by MSCs or their exosomes.[39,40] Therefore, we tested ETS2 expression, and the results of the luciferase and ChIP assays indicated that ETS2 expression was decreased in *ERK1*$^{-/-}$ BMMSCs, suggesting that ETS2, especially the ETS2-2- and ETS2-3-predicted binding sites on the *aurka* promoter region, transfers the signal from ERK1 to AURKA. Combining all the evidence, we demonstrated that ERK1, but not ERK2, induced T cell apoptosis via the ETS2/AURKA/NF-κB/Fas cascade.

In order to find a clinically applicable drug that can upregulate Erk1 expression, we focused on LA. A previous study has shown that LA was capable of upregulating ERK expression; however, whether LA could promote the capacity of MSCs in MSCT remained unclear.[22] The clinical safety of LA has already been proven in skin allergy and cancer clinical trials.[41–43] We confirmed that LA promoted the expression and phosphorylation of the ERK/IκB/NF-κB/Fas cascade in MSCs *in vitro* and observed that LA-treated MSCs more effectively induced T cell apoptosis. By applying LA-treated MSCs on DSS and CIA mouse models, the results showed enhanced therapeutic efficiency of MSCT, characterized by upregulating the Treg/Th17 ratio and immunomodulatory ability. However, the results showed that LA promoted the activation of both ERK1 and ERK2, and we did not screen out a small-molecule compound that specifically enhanced ERK1 to improve the therapeutic efficiency of MSCT. This limitation may lead to higher doses of cells or drugs being needed to achieve the desired therapeutic effect, as well as unpredictable side effects.

In summary, we proved that ERK1, but not ERK2, governs the immunomodulatory properties of MSCs via the ETS/AURKA/NF-κB/Fas/MCP-1 cascade. LA promotes the immunomodulatory properties of MSCs by activating the ERK cascade. LA treatment of MSCs may be a promising method to improve MSCT efficacy on ADs.

Limitations of the study

In this study, results suggested that LA promoted the activation of both ERK1 and ERK2, and we did not screen out a small-molecule compound that specifically enhanced ERK1 to improve the therapeutic efficiency of MSCT, which may lead to higher doses of the cells or drugs needed to achieve the desired therapeutic effect, as well as unpredictable side effects.

STAR★METHODS

Detailed methods are provided in the online version of this paper and include the following:

- KEY RESOURCES TABLE
- RESOURCE AVAILABILITY
  - Lead contact
  - Materials availability
  - Data and code availability
- EXPERIMENTAL MODEL AND STUDY PARTICIPANT DETAILS
  - Animal
  - Ethic
  - Isolation and expansion of bone marrow mesenchymal stem cells (BMMSCs)
  - Isolation, expansion and culture of umbilical cord mesenchymal stem cells (UCMSCs)
  - Cell-surface marker analysis of BMMSCs and UCMSCs
  - Isolation, culture and activation of T cells
- METHOD DETAILS
  - T cell migration assay
  - Apoptosis assay by flow cytometry
  - Flow cytometry analysis
  - Western Blot analysis
  - Cytokine array
  - Luciferase assay
  - ChIP assay
  - Establishment of dextran sodium sulphate (DSS)-induced colitis model and treatment by injection of MSCs
  - Establishment of collagen-induced arthritis (CIA) model and treatment by injection of human UCMSCs
  - Histological analysis on DSS model
  - Micro-CT analysis
  - Histological analysis on CIA model
- QUANTIFICATION AND STATISTICAL ANALYSIS
  - Disease activity index (DAI) on DSS model
  - Disease severity score on CIA model

- Statistical analysis
- ADDITIONAL RESOURCES

SUPPLEMENTAL INFORMATION

Supplemental information can be found online at https://doi.org/10.1016/j.isci.2023.107868.

ACKNOWLEDGMENTS

This work was supported by grants from the National Key Research and Development Program of China (2021YFA1100600 to Bei Li), the National Natural Science Foundation of China (81991504 to Bei Li), and the National Institute of Dental and Craniofacial Research (R00DE025915 and R03DE028026 to Chider Chen).

AUTHOR CONTRIBUTIONS

Qing Zhang: Conception and design, execution, collection and assembly of data, data analysis and interpretation, manuscript writing.
Xiao Lei: Execution, collection and assembly of data, data analysis and interpretation.
Fang Wang: Collection and assembly of data, data analysis and interpretation, manuscript writing.
Xiaoning He: Execution, collection of data.
Lu Liu: Execution, collection of data.
Yuxia Hou: data analysis and interpretation.
Yuan Liu: Execution, collection of data.
Fang Jin: Conception and design, administrative support, provision of study material.
Chider Chen: Conception and design, financial support, provision of study material, final approval of manuscript.
Bei Li: Conception and design, financial support, administrative support, provision of study material, final approval of manuscript.

DECLARATION OF INTERESTS

The authors declare no competing interests.

INCLUSION AND DIVERSITY

We support inclusive, diverse, and equitable conduct of research.

Received: May 18, 2023
Revised: August 3, 2023
Accepted: September 6, 2023
Published: September 9, 2023

REFERENCES

1. Jacobson, D.L., Gange, S.J., Rose, N.R., and Graham, N.M. (1997). Epidemiology and estimated population burden of selected autoimmune diseases in the United States. Clin. Immunol. Immunopathol. *84*, 223–243. https://doi.org/10.1006/clin.1997.4412.
2. Eaton, W.W., Rose, N.R., Kalaydjian, A., Pedersen, M.G., and Mortensen, P.B. (2007). Epidemiology of autoimmune diseases in Denmark. J. Autoimmun. *29*, 1–9. https://doi.org/10.1016/j.jaut.2007.05.002.
3. Wang, L., Wang, F.S., and Gershwin, M.E. (2015). Human autoimmune diseases: a comprehensive update. J. Intern. Med. *278*, 369–395. https://doi.org/10.1111/joim.12395.
4. Joensuu, J.T., Huoponen, S., Aaltonen, K.J., Konttinen, Y.T., Nordström, D., and Blom, M. (2015). The cost-effectiveness of biologics for the treatment of rheumatoid arthritis: a systematic review. PLoS One *10*, e0119683. https://doi.org/10.1371/journal.pone.0119683.
5. Castro-Manrreza, M.E., and Montesinos, J.J. (2015). Immunoregulation by mesenchymal stem cells: biological aspects and clinical applications. J. Immunol. Res. *2015*, 394917. https://doi.org/10.1155/2015/394917.
6. Munir, H., and McGettrick, H.M. (2015). Mesenchymal Stem Cell Therapy for Autoimmune Disease: Risks and Rewards. Stem Cells Dev. *24*, 2091–2100. https://doi.org/10.1089/scd.2015.0008.
7. Zhang, Q., Li, Q., Zhu, J., Guo, H., Zhai, Q., Li, B., Jin, Y., He, X., and Jin, F. (2019). Comparison of therapeutic effects of different mesenchymal stem cells on rheumatoid arthritis in mice. PeerJ *7*, e7023. https://doi.org/10.7717/peerj.7023.
8. Yang, Y., He, X., Zhao, R., Guo, W., Zhu, M., Xing, W., Jiang, D., Liu, C., and Xu, X. (2018). Serum IFN-gamma levels predict the therapeutic effect of mesenchymal stem cell transplantation in active rheumatoid arthritis. J. Transl. Med. *16*, 165. https://doi.org/10.1186/s12967-018-1541-4.
9. Carrion, F., Nova, E., Ruiz, C., Diaz, F., Inostroza, C., Rojo, D., Mönckeberg, G., and Figueroa, F.E. (2010). Autologous mesenchymal stem cell treatment increased T regulatory cells with no effect on disease activity in two systemic lupus erythematosus patients. Lupus *19*, 317–322. https://doi.org/10.1177/0961203309348983.
10. Zhu, M., Han, H., Hu, L., Cao, Y., and Fan, Z. (2022). Insulin-binding protein-5 down-regulates the balance of Th17/Treg. Front. Immunol. *13*, 1019248. https://doi.org/10.3389/fimmu.2022.1019248.
11. Tan, A.H.M., and Lam, K.P. (2010). Pharmacologic inhibition of MEK-ERK signaling enhances Th17 differentiation. J. Immunol. *184*, 1849–1857. https://doi.org/10.4049/jimmunol.0901509.
12. Cao, J., Zhang, X., Wang, Q., Wang, X., Jin, J., Zhu, T., Zhang, D., Wang, W., Li, X., Li, Y., et al. (2013). Cyclic AMP suppresses TGF-beta-mediated adaptive Tregs differentiation through inhibiting the activation of ERK and JNK. Cell. Immunol. *285*, 42–48. https://doi.org/10.1016/j.cellimm.2013.08.006.
13. Bai, X., Gou, X., Cai, P., Xu, C., Cao, L., Zhao, Z., Huang, M., and Jin, J. (2019). Sesamin Enhances Nrf2-Mediated Protective Defense against Oxidative Stress and Inflammation in Colitis via AKT and ERK Activation. Oxid.

Med. Cell. Longev. *2019*, 2432416. https://doi.org/10.1155/2019/2432416.
14. Wang, Z., Zhang, B., Wang, M., and Carr, B.I. (2005). Cdc25A and ERK interaction: EGFR-independent ERK activation by a protein phosphatase Cdc25A inhibitor, compound 5. J. Cell. Physiol. *204*, 437–444. https://doi.org/10.1002/jcp.20297.
15. Kajiya, M., Takeshita, K., Kittaka, M., Matsuda, S., Ouhara, K., Takeda, K., Takata, T., Kitagawa, M., Fujita, T., Shiba, H., and Kurihara, H. (2014). BDNF mimetic compound LM22A-4 regulates cementoblast differentiation via the TrkB-ERK/Akt signaling cascade. Int. Immunopharmacol. *19*, 245–252. https://doi.org/10.1016/j.intimp.2014.01.028.
16. Zhang, X., Qiu, J., Wang, H., Lu, Z., Shao, S., He, J., and Shen, Z. (2022). Autologous Bioactive Compound Concentrated Growth Factor Ameliorates Fistula Healing of Anal Fistula in a Pig Model and Promotes Proliferation and Migration of Human Skin Fibroblasts via Regulating the MEK/ERK Pathway. Oxid. Med. Cell. Longev. *2022*, 7660118. https://doi.org/10.1155/2022/7660118.
17. Chen, C., Akiyama, K., Yamaza, T., You, Y.O., Xu, X., Li, B., Zhao, Y., and Shi, S. (2014). Telomerase governs immunomodulatory properties of mesenchymal stem cells by regulating FAS ligand expression. EMBO Mol. Med. *6*, 322–334. https://doi.org/10.1002/emmm.201303000.
18. Akiyama, K., Chen, C., Wang, D., Xu, X., Qu, C., Yamaza, T., Cai, T., Chen, W., Sun, L., and Shi, S. (2012). Mesenchymal-stem-cell-induced immunoregulation involves FAS-ligand-/FAS-mediated T cell apoptosis. Cell Stem Cell *10*, 544–555. https://doi.org/10.1016/j.stem.2012.03.007.
19. Kühnel, F., Zender, L., Paul, Y., Tietze, M.K., Trautwein, C., Manns, M., and Kubicka, S. (2000). NFkappaB mediates apoptosis through transcriptional activation of Fas (CD95) in adenoviral hepatitis. J. Biol. Chem. *275*, 6421–6427. https://doi.org/10.1074/jbc.275.9.6421.
20. Briassouli, P., Chan, F., Savage, K., Reis-Filho, J.S., and Linardopoulos, S. (2007). Aurora-A regulation of nuclear factor-kappaB signaling by phosphorylation of IkappaBalpha. Cancer Res. *67*, 1689–1695. https://doi.org/10.1158/0008-5472.CAN-06-2272.
21. Karthigeyan, D., Prasad, S.B.B., Shandilya, J., Agrawal, S., and Kundu, T.K. (2011). Biology of Aurora A kinase: implications in cancer manifestation and therapy. Med. Res. Rev. *31*, 757–793. https://doi.org/10.1002/med.20203.
22. Ming, L., Jin, F., Huang, P., Luo, H., Liu, W., Zhang, L., Yuan, W., Zhang, Y., and Jin, Y. (2014). Licochalcone A up-regulates of FasL in mesenchymal stem cells to strengthen bone formation and increase bone mass. Sci. Rep. *4*, 7209. https://doi.org/10.1038/srep07209.
23. Zhang, S., Chuah, S.J., Lai, R.C., Hui, J.H.P., Lim, S.K., and Toh, W.S. (2018). MSC exosomes mediate cartilage repair by enhancing proliferation, attenuating apoptosis and modulating immune reactivity. Biomaterials *156*, 16–27. https://doi.org/10.1016/j.biomaterials.2017.11.028.
24. Coleman, M.A., and Steptoe, R.J. (2012). Induction of antigen-specific tolerance through hematopoietic stem cell-mediated gene therapy: the future for therapy of autoimmune disease? Autoimmun. Rev. *12*, 195–203. https://doi.org/10.1016/j.autrev.2011.08.012.
25. Siatskas, C., Chan, J., Field, J., Murphy, K., Nasa, Z., Toh, B.H., and Alderuccio, F. (2006). Gene therapy strategies towards immune tolerance to treat the autoimmune diseases. Curr. Gene Ther. *6*, 45–58. https://doi.org/10.2174/156652306775515600.
26. Buscà, R., Pouysségur, J., and Lenormand, P. (2016). ERK1 and ERK2 Map Kinases: Specific Roles or Functional Redundancy? Front. Cell Dev. Biol. *4*, 53. https://doi.org/10.3389/fcell.2016.00053.
27. Lloyd, A.C. (2006). Distinct functions for ERKs? J. Biol. *5*, 13. https://doi.org/10.1186/jbiol46.
28. Jones, F.K., Stefan, A., Kay, A.G., Hyland, M., Morgan, R., Forsyth, N.R., Pisconti, A., and Kehoe, O. (2020). Syndecan-3 regulates MSC adhesion, ERK and AKT signalling in vitro and its deletion enhances MSC efficacy in a model of inflammatory arthritis in vivo. Sci. Rep. *10*, 20487. https://doi.org/10.1038/s41598-020-77514-z.
29. Xiong, H., Guo, Z., Tang, Z., Ai, X., Qi, Q., Liu, X., Huang, D., Li, Z., Ji, S., and Guo, Q. (2020). Mesenchymal Stem Cells Activate the MEK/ERK Signaling Pathway and Enhance DNA Methylation via DNMT1 in PBMC from Systemic Lupus Erythematosus. BioMed Res. Int. *2020*, 4174082. https://doi.org/10.1155/2020/4174082.
30. Blázquez-Prunera, A., Almeida, C.R., and Barbosa, M.A. (2019). Fibroblast growth factor improves the motility of human mesenchymal stem cells expanded in a human plasma-derived xeno-free medium through alphaVbeta3 integrin. J. Tissue Eng. Regen. Med. *13*, 36–45. https://doi.org/10.1002/term.2766.
31. Liu, Y., Jing, H., Kou, X., Chen, C., Liu, D., Jin, Y., Lu, L., and Shi, S. (2018). PD-1 is required to maintain stem cell properties in human dental pulp stem cells. Cell Death Differ. *25*, 1350–1360. https://doi.org/10.1038/s41418-018-0077-8.
32. Gu, Y.Z., Xue, Q., Chen, Y.J., Yu, G.H., Qing, M.D., Shen, Y., Wang, M.Y., Shi, Q., and Zhang, X.G. (2013). Different roles of PD-L1 and FasL in immunomodulation mediated by human placenta-derived mesenchymal stem cells. Hum. Immunol. *74*, 267–276. https://doi.org/10.1016/j.humimm.2012.12.011.
33. Böcker, W., Docheva, D., Prall, W.C., Egea, V., Pappou, E., Rossmann, O., Popov, C., Mutschler, W., Ries, C., and Schieker, M. (2008). IKK-2 is required for TNF-alpha-induced invasion and proliferation of human mesenchymal stem cells. J. Mol. Med. *86*, 1183–1192. https://doi.org/10.1007/s00109-008-0378-3.
34. Dorronsoro, A., Ferrin, I., Salcedo, J.M., Jakobsson, E., Fernández-Rueda, J., Lang, V., Sepulveda, P., Fechter, K., Pennington, D., and Trigueros, C. (2014). Human mesenchymal stromal cells modulate T-cell responses through TNF-alpha-mediated activation of NF-kappaB. Eur. J. Immunol. *44*, 480–488. https://doi.org/10.1002/eji.201343668.
35. Raicevic, G., Najar, M., Busser, H., Crompot, E., Bron, D., Toungouz, M., and Lagneaux, L. (2017). Comparison and immunobiological characterization of retinoic acid inducible gene-I-like receptor expression in mesenchymal stromal cells. Sci. Rep. *7*, 2896. https://doi.org/10.1038/s41598-017-02850-6.
36. Deng, P., Zhou, C., Alvarez, R., Hong, C., and Wang, C.Y. (2016). Inhibition of IKK/NF-kappaB Signaling Enhances Differentiation of Mesenchymal Stromal Cells from Human Embryonic Stem Cells. Stem Cell Rep. *6*, 456–465. https://doi.org/10.1016/j.stemcr.2016.02.006.
37. Furukawa, T., Kanai, N., Shiwaku, H.O., Soga, N., Uehara, A., and Horii, A. (2006). AURKA is one of the downstream targets of MAPK1/ERK2 in pancreatic cancer. Oncogene *25*, 4831–4839. https://doi.org/10.1038/sj.onc.1209494.
38. Luo, Y., Jiang, N., May, H.I., Luo, X., Ferdous, A., Schiattarella, G.G., Chen, G., Li, Q., Li, C., Rothermel, B.A., et al. (2021). Cooperative Binding of ETS2 and NFAT Links Erk1/2 and Calcineurin Signaling in the Pathogenesis of Cardiac Hypertrophy. Circulation *144*, 34–51. https://doi.org/10.1161/CIRCULATIONAHA.120.052384.
39. Islas, J.F., Abbasgholizadeh, R., Dacso, C., Potaman, V.N., Navran, S., Bond, R.A., Iyer, D., Birla, R., and Schwartz, R.J. (2020). beta-Adrenergic stimuli and rotating suspension culture enhance conversion of human adipogenic mesenchymal stem cells into highly conductive cardiac progenitors. J. Tissue Eng. Regen. Med. *14*, 306–318. https://doi.org/10.1002/term.2994.
40. Sutter, W., Stein, E., Koehn, J., Schmidl, C., Lezaic, V., Ewers, R., and Turhani, D. (2009). Effect of different biomaterials on the expression pattern of the transcription factor Ets2 in bone-like constructs. J. Cranio-Maxillo-Fac. Surg. *37*, 263–271. https://doi.org/10.1016/j.jcms.2009.01.007.
41. Weber, T.M., Ceilley, R.I., Buerger, A., Kolbe, L., Trookman, N.S., Rizer, R.L., and Schoelermann, A. (2006). Skin tolerance, efficacy, and quality of life of patients with red facial skin using a skin care regimen containing Licochalcone A. J. Cosmet. Dermatol. *5*, 227–232. https://doi.org/10.1111/j.1473-2165.2006.00261.x.
42. Wanitphakdeedecha, R., Tavechodperathum, N., Tantrapornpong, P., Suphatsathienkul, P., Techapichetvanich, T., Eimpunth, S., and Manuskiatti, W. (2020). Acne treatment efficacy of intense pulsed light photodynamic therapy with topical licochalcone A, l-carnitine, and decanediol: A spilt-face, double-blind, randomized controlled trial. J. Cosmet. Dermatol. *19*, 78–87. https://doi.org/10.1111/jocd.13178.
43. Puaratanaarunkon, T., and Asawanonda, P. (2022). A Randomized, Double Blinded, Split-Face Study of the Efficacy of Using a Broad Spectrum Sunscreen with Anti-Inflammatory Agent to Reduce Post Inflammatory Hyperpigmentation After Picosecond Laser. Clin. Cosmet. Investig. Dermatol. *15*, 331–337. https://doi.org/10.2147/CCID.S355329.
44. Yang, X., Zhou, F., Yuan, P., Dou, G., Liu, X., Liu, S., Wang, X., Jin, R., Dong, Y., Zhou, J., et al. (2021). T cell-depleting nanoparticles ameliorate bone loss by reducing activated T cells and regulating the Treg/Th17 balance. Bioact. Mater. *6*, 3150–3163. https://doi.org/10.1016/j.bioactmat.2021.02.034.
45. Ezzatollah Fathi, B.V., and Farahzadi, R. (2020). Targeting the Proliferation Inhibition of Chronic Myeloid Leukemia Cells by Bone Marrow Derived-

Mesenchymal Stem Cells via ERK Pathway as a Therapeutic Strategy. Acta Med. Iran. *58*, 5.

46. Fathi, E., Vandghanooni, S., Montazersaheb, S., and Farahzadi, R. (2021). Mesenchymal stem cells promote caspase-3 expression of SH-SY5Y neuroblastoma cells via reducing telomerase activity and telomere length. Iran. J. Basic Med. Sci. *24*, 1583–1589. https://doi.org/10.22038/IJBMS.2021.59400.13187.

47. Xin, L., Zhou, F., Zhang, C., Zhong, W., Xu, S., Jing, X., Wang, D., Wang, S., Chen, T., and Song, J. (2022). Four-Octyl itaconate ameliorates periodontal destruction via Nrf2-dependent antioxidant system. Int. J. Oral Sci. *14*, 27. https://doi.org/10.1038/s41368-022-00177-1.

48. Qi, M., Zhang, L., Ma, Y., Shuai, Y., Li, L., Luo, K., Liu, W., and Jin, Y. (2017). Autophagy Maintains the Function of Bone Marrow Mesenchymal Stem Cells to Prevent Estrogen Deficiency-Induced Osteoporosis. Theranostics *7*, 4498–4516. https://doi.org/10.7150/thno.17949.

49. Chen, W., Wang, J., Xu, Z., Huang, F., Qian, W., Ma, J., Wee, H.B., Lewis, G.S., June, R.R., Schafer, P.H., et al. (2018). Apremilast Ameliorates Experimental Arthritis via Suppression of Th1 and Th17 Cells and Enhancement of CD4(+)Foxp3(+) Regulatory T Cells Differentiation. Front. Immunol. *9*, 1662. https://doi.org/10.3389/fimmu.2018.01662.

STAR★METHODS

KEY RESOURCES TABLE

REAGENT or RESOURCE	SOURCE	IDENTIFIER
Antibodies		
Anti-CD28 antibody	eBioscience	Cat # 14-0281-82; RRID: AB_467190
Anti-CD3ε antibody	BioLegend	Cat # 100301; RRID: AB_312666
Anti-CD3-APC antibody	BioLegend	Cat # 100235; RRID: AB_2561455
Anti-CD4-PE/Cy7 antibody	BioLegend	Cat # 100421; RRID: AB_312706
Anti-CD25-APC antibody	BioLegend	Cat # 101909; RRID: AB_961208
Anti-Foxp3-PE antibody	eBioscience	Cat # 12-5773-82; RRID: AB_465936
Anti-IL-17-PE antibody	eBioscience	Cat # 12-7177-81; RRID: AB_763582
Anti-Fas antibody	Santa Cruz Biotechnology	Cat # sc-74540; RRID: AB_1121387
Anti-Fas ligand antibody	Santa Cruz Biotechnology	Cat # sc-19681; RRID: AB_626940
Anti-NFκB antibody	Cell signaling Technology	Cat # 8242T; RRID: AB_10859369
Anti-*p*-NFκB antibody	Cell signaling Technology	Cat # 3031S; RRID: AB_330559
Anti-IKB antibody	Cell signaling Technology	Cat # 4814T; RRID: AB_390781
Anti-p-IKB antibody	Cell signaling Technology	Cat # 2859T; RRID: AB_561111
Anti-AURKA antibody	Cell signaling Technology	Cat # 91590S; RRID: AB_2800171
Anti-p-AURKA antibody	Cell signaling Technology	Cat # 2914S; RRID: AB_2061631
Anti-ETS2 antibody	Cell signaling Technology	Cat # 66476S; RRID: AB_2799711
Anti-ERK antibody	Cell signaling Technology	Cat # 4695S; RRID: AB_390779
Anti-p-ERK antibody	Cell signaling Technology	Cat # 4370S; RRID: AB_2315112
FITC- Goat Anti-Rabbit IgG	Yeasen	Cat # 33107ES60
Biological samples		
Umbilical cord tissue & UCMSCs	Northwest Women's and Children's Hospital	N/A
Chemicals, peptides, and recombinant proteins		
pGL3-basic vector	Promega	Cat # E-1751
Dual-Glo Luciferase system	Promega	Cat # E2920
DSS	MP Biomedicals	Cat # 9011-18-1
type II collagen (CII)	Chondrex	Cat # 20062
Licochalcone A	Sigma	Cat # PHL80486
U0126	Cell Signaling Technology	Cat # 9903S
Critical commercial assays		
PE Annexin V Apoptosis Detection Kit I	BD Bioscience	Cat # 559763
cytokine array kit	R&D Systems	Cat # ARY006
ChIP assay kit	Millipore	Cat # 17-295
True-Nuclear Transcription Factor Buffer Set	BioLegend	Cat # 424401
Experimental models: Organisms/strains		
Mouse:ERK1-/-:B6.129(Cg)-Mapk3tm1Gela/J	Jackson Laboratory, USA	N/A
Mouse: ERK2-/-:B6.129-Mapk1tm1Gela/J	Jackson Laboratory, USA	N/A
Mouse:Fas-/-:C3MRL-Faslpr/J	Jackson Laboratory, USA	N/A
DBA/1 mice	Beijing Vital River Laboratory, China	N/A

(*Continued on next page*)

Continued

REAGENT or RESOURCE	SOURCE	IDENTIFIER
Software and algorithms		
Micview V2.1.2	Chen et al.[49]	https://doi.org/10.3389/fimmu.2018.01662
GraphPad Prism 6	GraphPad Software	RRID:SCR_002798
Other		
CHIP assay data	This paper	Table S1

RESOURCE AVAILABILITY

Lead contact

Further information and requests for resources and reagents should be directed to and will be fulfilled by the lead contact, Bei Li (libei2021@fmmu.edu.cn).

Materials availability

This study did not generate new unique reagents.

Data and code availability

- The data sets generated during and/or analyzed during the current study are available from the corresponding author upon reasonable request.
- ChIP assay of Ets2/Aurka raw data and original western blot images are available in the Supplemental information. Other data reported in this paper will be shared by the lead contact upon request.
- This paper does not report original code, software, or algorithm.
- Any additional information required to reanalyze the data reported in this paper is available from the lead contact upon request.

EXPERIMENTAL MODEL AND STUDY PARTICIPANT DETAILS

Animal

B6.129(Cg)-*Mapk3*^{tm1Gela}/J (*ERK1*$^{-/-}$), B6.129-*Mapk1*^{tm1Gela}/J(*ERK2*$^{-/-}$), and C3MRL-Fas^{lpr}/J mice (*Fas*$^{-/-}$) mice were purchased from the Jackson Laboratory, Maine, USA. Male C57BL/6 mice were purchased from the Animal Center of Fourth Military Medical University, Xi'an, China. DBA/1 mice were purchased from Beijing Vital River Laboratory in Beijing, China. For all the *ERK1*$^{-/-}$, *ERK2*$^{-/-}$ and *Fas*$^{-/-}$ mice involved in cell extraction, the sex were evenly distributed between males and females. For C57BL/6 and DBA/1 mice involved in cell extraction and DSS/CIA modeling, they are both male in sex. The potential consequences of gender differences are not discussed in this study and need to be further explored. All mice were 8-week-old and were housed four to five per cage under specific pathogen-free conditions (22°C, 50%–55% humidity, 12 h light/12 h dark cycles, and *ad libitum* access to food and water) for 2 weeks prior to experimentation. All experimental procedures have been approved by the Animal Protection Committee of the Fourth Military Medical University, China. Animal welfare and experimental procedures were complied with the principles of *Laboratory animal – Guidelines for ethical review of animal welfare* (GB/T 35892–2018).

Ethic

UCMSCs were isolated from the umbilical cord tissue of patients from the Northwest Women's and Children's Hospital. The study was conducted in accordance with the Declaration of Helsinki, and the protocol was approved by the local research ethics committee (authorization number: 2022-612). Informed consent to use the discarded surgical tissue for research purposes was signed by all the enrolled patients.

Isolation and expansion of bone marrow mesenchymal stem cells (BMMSCs)

Primary BMMSCs were drawn out by flushing from tibias and femurs of *ERK1*$^{-/-}$, *ERK2*$^{-/-}$ and *Fas*$^{-/-}$ mice with basal culture medium containing α-MEM medium (Gibco, NY, USA), 20% FBS (Sijiqing, Hangzhou, China), 2 mM L-glutamine (Invitrogen, Carlsbad, CA), 100 U/mL penicillin and 100 U/mL streptomycin (Invitrogen, Carlsbad, CA). Single-cell suspension was equally seeded in 10 cm dishes (Thermo, Suzhou, China) and initially maintained in an atmosphere of 5% CO_2 at 37°C. The medium was changed every 2 days until the adherent cells were 80–90% confluent. Then BMMSCs were passaged after digestion with 0.25% trypsin. Third and fourth passage cells were used for experiments.[17]

Isolation, expansion and culture of umbilical cord mesenchymal stem cells (UCMSCs)

Human UCMSCs were provided by the Northwest Women's and Children's Hospital in Xi an, China. The use of human UCMSCs in this study was approved by the local Ethics Committee, following the *Guidelines for Human Embryonic Stem Cell Research (2005)*. The umbilical cords

were collected from 10 pregnant Chinese women with 24, 25, 30, 30, 30, 32, 33, 34, 34, and 36 years old. Samples were cut into segments (2-3 cm) after rinsed several times in sterile PBS. Cord vessels, including 2 arteries and 1 vein, were removed. Then the umbilical cords were cut into small pieces (0.5-1 cm^3) and placed directly into 10 cm culture dishes for culture expansion in α-MEM culture medium supplemented with 10% FBS in an atmosphere of 5% CO_2 at 37°C. After 5 days, non-adherent cells were discarded, and adherent cells were continued to culture. The medium was changed every 2 days until the adherent cells were 80–90% confluent. Then UCMSCs were passaged after digestion with 0.25% trypsin. Third and fourth passage cells were used for experiments. 0.1 mM LA (Sigma, USA) or 10 μM U0126 (Cell Signaling Technology, MA, USA) were added in culture medium respectively for 12 h to culture LA-UCMSC and U0126-UCMSC.[7]

Cell-surface marker analysis of BMMSCs and UCMSCs

Mouse BMMSCs was incubated with anti-mouse CD105-PE, CD73-FITC, CD45-PE, CD34-PE and Sca-1-FITC (all from eBioscience, USA) respectively for 30 min in the dark at 4°C. Human UCMSCs were incubated with anti-human CD105-PE, CD73-FITC-, CD90-PE, CD45-PE, CD34-PE, CD14-FITC, CD19-APC, and HLA-DR-FITC (all from eBioscience, USA) respectively under the same condition as mouse BMMSCs. Afterward, the cells were then washed and suspended for flow cytometry analysis.[7,17]

Isolation, culture and activation of T cells

Spleens from male C57BL/6 mice were harvested and single-cell suspension was prepared by crushing spleens on 70 μm cell strainers. Cell suspension was cultured in in RPMI 1640 medium (Gibco, NY, USA) supplemented with 10% FBS (Sijiqing, Hangzhou, China), 50 mM 2-mercaptoethanol, 2 mM L-glutamine (Sigma-Aldrich, USA), and 1% penicillin/streptomycin (Invitrogen, USA) after purified by red blood cell lysis buffer (Yeasen, Shanghai, China). Cells cultured in RPMI 1640 medium with anti-CD28 antibody (2 μg/mL) (eBioscience, USA) were seeded in plate which was pre-coated with anti-CD3ε antibody (5 μg/mL in PBS) (BioLegend, USA) at 37°C for 4 h. T cells were activated after 48 h of incubation.[44]

METHOD DETAILS

T cell migration assay

A transwell system was used for T cell migration assay. 2×10^5 bone marrow mesenchymal stem cells (BMMSCs) stained by PKH26 (Invitrogen Life Technology, USA) were seeded on the lower chamber of a 12-well culture plate with transwell and incubated for 24 h. The prestimulated T cells with anti-CD3ε and anti-CD28 antibodies (both from eBioscience, USA) for 48 h were loaded onto the upper chamber of transwell and co-cultured for 48 h, followed by observation under a fluorescent microscope. Green-labeled cell number was counted and normalized by red-labeled number of BMMSCs in five representative images.[18]

Apoptosis assay by flow cytometry

1×10^5 MSCs were seeded on a 6-well culture plate and incubated for 24 h. 1×10^6 pre-activated T cells were directly loaded in 6-well culture plate and co-cultured with MSCs for 24 h. T cells were stained by anti-CD3-APC antibody (BioLegend, USA) for 30 min and then stained by PE Annexin V and 7-AAD (BD Biosciences, USA) for 15 min. T cell apoptosis was detected analyzed with flow cytometer.[17]

Flow cytometry analysis

T cells was stained with anti-CD4-PE/Cy7 antibody (BioLegend, USA) or anti-CD25-APC antibody (BioLegend, USA) for 30 min. After fixation and permeabilization with a True-Nuclear Transcription Factor Buffer Set (BioLegend, USA), T cells were stained with anti-Foxp3-PE antibody (eBioscience, USA) for detection of Tregs. T cells were incubated with Cell Activation Cocktail (BioLegend, USA) and Anti-IL-17-PE antibody (eBioscience, USA) for detection of Th17 cells.[44] The protocol for detecting the expression of ERK1/2 were carried out according to Ezzatollah Fathi BV et al.[45]

Western Blot analysis

Radioimmunoprecipitation assay (RIPA) buffer (Beyotime Biotechnology, Shanghai, China) with protease inhibitor were used to extract protein from MSCs. Bicinchoninic Acid (BCA) quantitative assay kit (Beyotime Biotechnology, Shanghai, China) was used to measure the protein concentration. Twenty microgram protein was separated by 10 – 12% Tris-glycine sodium dodecyl sulfatepolyacrylamide gel (Invitrogen Life Technology, USA), followed by transferred onto a polyvinylidene fluoride membrane (Millipore, USA). Blocking was performed by using 5% Bovine Serum Albumin (BSA) for 2 h at room temperature. The membrane was incubated with primary antibodies overnight at 4°C. Antibodies against Fas (Santa Cruz Biotechnology, USA), Fas ligand (FasL) (Santa Cruz Biotechnology, USA), NFκB (Cell signaling, USA), p-NFκB (Cell signaling, USA), IKB (Cell signaling, USA), p-IKB (Cell signaling, USA), AURKA (Cell signaling, USA), p-AURKA (Cell signaling, USA), ETS2 (Cell signaling, USA), ERK (Cell signaling, USA), p-ERK (Cell signaling, USA), GAPDH (Abbiotec, USA), and β-actin (Abbiotec, USA) were used. Secondary antibodies (Jackson ImmunoResearch, PA, USA) were incubated for 2 h at room temperature. The protein accumulation was detected by Western-light Chemiluminescent Detection System (Peiqing, Shanghai, China).[46] Uncropped images is shown in Figure S3.

Cytokine array

Cell supernatant was centrifuged at 1500 g for 15 min. The sICAM, IFNγ, CXCL10, CXCL1, MCSF, MCP-1, and CCL4 concentrations in the cell supernatant were determined by cytokine array kit (R&D Systems, Minnesota, USA) according to the manufacturer's protocol.[47]

Luciferase assay

Aurka-luciferase promoter reporter construct was generated by PCR with Pfu polymerase and mouse genomic DNA as a template. Primers containing XhoI and HindIII restriction sites were used to amplify *Aurka* promoter fragments (~1 kb construct: forward, 5′-CTCGAGCTCCA-GAGCCCAGAACTT AAC-3′ and reverse, 5′-AAGCTTTCAACAGCCATGTCCCTTTC-3′). XhoI and HindIII digested PCR products were subcl-oned into a pGL3-basic vector (Promega, USA). Point mutations on ETS2 binding sites were introduced into the reporter by the Pfu/DpnI method. All clones were confirmed by sequencing on both strands. MSCs cultured in 6-well plates were transfected with 2 μg luciferase re-porter and 100 ng Renilla luciferase expression vector. At 48 hours post-transfection, cells were lysed in passive lysis buffer and luciferase ac-tivity was detected using the Dual-Glo Luciferase system (Promega, USA) with luminometer (Turner Designs, USA).[17]

ChIP assay

ChIP assay was performed using a ChIP assay kit (Millipore, California, USA). BMMSCs was fixed with formaldehyde/phosphate-buffered saline and sonicated to obtain DNA fragments. Chromatin fragments were incubated overnight at 4°C with anti-Ets2 antibody (Cell Signaling, MA, USA), and bound DNA precipitants were analyzed using PCR.[17] The primers of ETS2 were forward-1, 5′-CTCCAGAGCCCAGAACT-TAAC-3′ and reverse-1, 5′-GTAAAGGCTCAACCTCCTTCTC-3′; forward-2, 5′-ACTTCCAATGGGACACAGATAA-3′ and reverse-2, 5′-GCTAA CGGAGAGGAT GGC-3′; forward-3, 5′-TGATCCACTACAGACCCTAGC-3′ and reverse-3, 5′-CACGATTCG CTCCTCCATTT-3′; forward-4, 5′-GATCGATCGCTCGGAGT-3′ and reverse-4, 5′-CCCAGG ATCAGGCGTTC-3′; forward-5, 5′-GATAGAACGGCCGCAGAT-3′ and reverse-5, 5′-TAGGAG TCAAACCCTCTACTCC-3′; forward-6, 5′-GGAGTAGAGGGTTTGACTCCTA-3′ and reverse-6, 5′-TCAACAGCCATG TCCCTTTC-3′.

Establishment of dextran sodium sulphate (DSS)-induced colitis model and treatment by injection of MSCs

A total of twenty-five male C57BL/6 mice were randomly assigned to five experimental groups: control group (Control), DSS treatment group (DSS), DSS mice infused with wild-type BMMSCs group (WT), DSS mice infused with *ERK1*$^{-/-}$ BMMSCs groups (ERK1$^{-/-}$) and DSS mice infused with *ERK2*$^{-/-}$ BMMSCs group (ERK2$^{-/-}$). Experimental colitis was induced by feeding mice with 3% w/v DSS (MP Biomedicals, CA, USA) in drink-ing water. Control mice received drinking water without DSS. On day 3, 1×10^6 BMMSCs from WT mice, *ERK1*$^{-/-}$ mice, and *ERK2*$^{-/-}$ mice were dissolved in 200 μL PBS per mouse and infused via tail vein. An equal volume of PBS was administered to Control and DSS groups. All mice were sacrificed at day 10.[48]

A total of thirty male C57BL/6 mice were randomly assigned to five experimental groups: control group (Control), DSS treatment group (DSS), DSS mice infused with UCMSCs (UCMSC) group, DSS mice infused with U0126 treated UCMSCs (U0126-UCMSC) group and DSS mice infused with LA treated UCMSCs (LA-UCMSC) group. All mice were fed the same food. The mice in the control group were fed with tri-distilled water. Experimental colitis was induced by feeding mice with 3% w/v DSS (MP Biomedicals, CA, USA) in drinking water. On day 3, 1×10^6 hu-man UCMSCs after different treatments (see "isolation, expansion and culture of umbilical cord mesenchymal stem cells" in Experimental model and subject detail) dissolved in 200 μL PBS per mouse were infused via tail vein to UCMSC, U0126-UCMSC and LA-UCMSC group, and an equal volume of PBS was administered to Control group and DSS group.

Establishment of collagen-induced arthritis (CIA) model and treatment by injection of human UCMSCs

Thirty male DBA/1 mice were randomly assigned to five experimental groups: control group (Control), CIA mice group (CIA), CIA mice infused with UCMSCs group (UCMSC), CIA mice infused with U0126-UCMSCs group (U0126-UCMSC), and CIA mice infused with LA-UCMSCs group (LA-UCMSC). CIA mice received an injection into the base of the tail with 100 μg of type II collagen (CII) (Chondrex; MD Biosciences) emul-sified in Freund's complete adjuvant. 15 days later, CIA mice received booster injections of 100 μg of type II collagen in Freund's incomplete adjuvant.[7] On day 30, 1×10^6 human UCMSCs after different treatments (see "isolation, expansion and culture of umbilical cord mesenchymal stem cells" in Experimental model and subject detail) dissolved in 200 μL PBS per mouse were infused via tail vein to three groups (UC, U0126 and LA groups) and an equal volume of PBS was administered to Control group and CIA group. All mice were sacrificed at day 60.

Histological analysis on DSS model

At day 10, all mice were killed and colons were removed. Colon tissues were fixed for 24 h in 4% paraformaldehyde at 4°C. The following day, colons were embedded in paraffin and serially sectioned into 3 μm thick paraffin sections. The sections were stained with haematoxylin–eosin (Leica Biosystems) using standard protocols. Sections were observed under the light microscope (DM6B; Leica). The histological activity index was graded according to following standard: normal colon mucosa received a score of 0, slight oedema and infiltration of inflammatory cells received a score of 1; loss of basal crypts with moderate inflammation in lamina propria received a score of 2; total loss of basal crypts with severe inflammation in lamina propria, but with surface epithelium still remaining received a score of 3; and loss of all crypts and surface epithelium with severe inflammation in the mucosa, muscularis propria and submucosa received a score of 4.[48]

Micro-CT analysis

All mice were sacrificed and mice hind limbs were cut off at day 60. Micro-CT scans of the hind limbs were performed using an explore Locus SP micro-CT scanner (GE, America) with the following scanning parameters: scanning resolution: 14 μm; rotation angle: 360°; tube voltage: 80 kV; tube current, 80 μA; exposure time, 2960ms; everage frame: 4; and pixel combination: 1×1. The software program Micview V2.1.2 and ABA were used to create a 3D reconstruction and to analyze the bone. The measured area of bone volume was set with a length of 1 mm in the distal and proximal direction from the center of each metatarsophalangeal joint. The mean bone volume of the second to fourth metatarsal and phalangeal bones were compared.[49]

Histological analysis on CIA model

Hind limbs were decalcified in 17% EDTA for 15 days after being fixed for 48 h in 4% paraformaldehyde at 4°C. Then hind limbs were embedded in paraffin and serially sectioned into 3 μm thick paraffin sections. The sections were stained with haematoxylin–eosin (Leica Biosystems) using standard protocols. Sections were observed under the light microscope (DM6B; Leica). The extent of synovitis, pannus formation, and bone/cartilage destruction was determined using a graded scale, as follows: no signs of inflammation received a score of 0, mild inflammation with hyperplasia of the synovial lining without cartilage destruction received a score of 1, increasing degrees of inflammatory cell infiltration and cartilage/bone destruction received a score of 2–4.[7]

QUANTIFICATION AND STATISTICAL ANALYSIS

Disease activity index (DAI) on DSS model

Weight loss, stool formation, and bloody stool for each mouse were calculated by grading on a scale of 0 – 4 respectively. The score for each mouse was represented as the sum of the weight loss, stool formation, and bloody stool at day 10.[48]

Disease severity score on CIA model

Each paw was evaluated for a period of every three days after the infusion of UCMSCs and were scored individually for the severity of arthritis using a previously described scoring system. No evidence of erythema and swelling received a score of 0, erythema and mild swelling confined to the tarsals or metatarsals received a score of 1, erythema and moderate swelling of tarsal and the metatarsal or tarsal and ankle joints received a score of 2, erythema and severe swelling extending from the ankle to metatarsal joints received a score of 3, and erythema and severe swelling encompassing the ankle, foot, and digits, or ankylosis of the limb received a score of 4. Four paws scores added up to a total score per mouse.[7]

Statistical analysis

All numerical data are expressed as mean ± standard deviation (SD) of five mice per group. Statistical analyses were performed using the Prism software version 6 (GraphPad, La Jolla, CA). Comparisons between means groups were analyzed using ordinary one-way ANOVA with Tukey's multiple comparisons test. $P < .05$ was considered significant. Statistical significance is indicated with $*P < .05$, $**P < .01$, $***P < .001$. Data are represented as mean +/- SEM in Figures.

ADDITIONAL RESOURCES

This study involves the collection of human umbilical cord, authorized by Ethics Committee of Xi'an Jiaotong University Medical Science Center with Research ethics approval documents available in the Supplemental information.